Early Events in Decatungstate Photocatalyzed Oxidations: A Nanosecond Laser Transient Absorbance Reinvestigation

Dean C. Duncan and Marye Anne Fox*

Department of Chemistry and Biochemistry, University of Texas at Austin, Austin, Texas 78712

Received: January 8, 1998; In Final Form: March 17, 1998

Transient absorbance changes following nanosecond flash excitation of $M_4[W_{10}O_{32}]$ ($M = Na^+$ or $(n\text{-}C_4H_9)_4N^+ \equiv Q^+$) in acetonitrile reveal a long-lived ligand-to-metal charge-transfer (LMCT) intermediate $[W_{10}O_{32}]^{4-\dagger}$ ($\phi \sim 0.50$, $\tau > 74$ ns) as the reactive species in photocatalyzed organic oxidations. From its long lifetime and the lack of detectable emission between 400 and 900 nm, this LMCT intermediate is assigned to a "hot" ground-state isomer which is quenched reductively to $[W_{10}O_{32}]^{5-}$ or its protonated derivative $[HW_{10}O_{32}]^{4-}$. Up to 1 μs after flash excitation of $Na_4[W_{10}O_{32}]$, the kinetics and quantum yields are measured for the reductive quenching of $[W_{10}O_{32}]^{4-\dagger}$ by thiocyanate and four classes of organic substrates. Aromatic amines, thianthrene, and thiocyanate quench $[W_{10}O_{32}]^{4-\dagger}$ by electron transfer at or near diffusion-controlled rates, and the alkanes and 2-butanol quench $[W_{10}O_{32}]^{4-\dagger}$ by hydrogen atom transfer with rate constants in the range 10^7-10^8 M^{-1} s^{-1}. High yields of the geminate pairs do not require photoexcitation of ground-state adducts, substrate- -$[W_{10}O_{32}]^{4-}$, but do require protonation of the reduction product $[W_{10}O_{32}]^{5-}$.

Introduction

Polyoxometalates (POMs) are discrete d^0 metal oxide complexes that exhibit a wide variety of alterable shapes, sizes, and surface charge densities.[1−5] The most striking properties of these complexes are their reversible multielectron reduction capacity, their wide range of tunable redox potentials, and their high oxidative and thermal stabilities.[1−5] Both the energetics and mechanism of the polyoxometalate-catalyzed functionalization of organic substrates have been addressed, centering on alcohols,[4,6−12] ketones,[13] amines,[6,14] and the activation of C−H bonds in saturated hydrocarbons.[13,15−23] Most of these reports rely on indirect techniques, e.g., organic product distributions or steady-state photochemical reaction kinetics and quantum yields.

In the photodehydrogenation of saturated hydrocarbons, product distributions can be controlled by varying the ground-state redox potential of the polyoxometalate involved in the thermal "dark" reactions subsequent to the primary photochemical event. In particular, highly oxidizing polyoxometalates (e.g., α-$[PW_{12}O_{40}]^{3-}$) exclusively produce the more highly substituted (thermodynamic) alkenes, which is consistent with carbenium ion intermediates.[19] With less oxidizing polyoxometalates (e.g., $[W_{10}O_{32}]^{4-}$), however, the least substituted (nonthermodynamic) alkenes and dimers are produced, as is consistent with disproportionation and dimerization of radical intermediates.[19] In radicals for which dimerization and disproportionation are disfavored by steric factors (e.g., the adamantyl radical), methyl ketones are produced, probably through an intermediate carbanion.[24] However, there is little direct evidence on the substrate-activating events, on the identity of key intermediates, on the relative efficiencies of thermal back reactions within solvent cages and from freely diffusing intermediates, or on the limiting quantum yields of primary and secondary products.[8,9,22,23] Nor is it understood which of these processes control the course of polyoxometalate photocatalyzed dehydrogenations.

In an attempt to address these questions, $M_4[W_{10}O_{32}]$ (M_4**1**, $M = Na^+$ or $Q^+ \equiv (n\text{-}C_4H_9)_4N^+$) was chosen for further investigation for two reasons. First, the known electronic spectra and molar absorptivities of the one- and two-electron reduced species permit clarification of their involvement in photochemical transformations of M_4**1**.[25−27] Second, picosecond,[23,28] and nanosecond[22,28,29] transient absorbance studies of M_4**1** have been reported.

SCHEME 1: Intermediates Generated by Flash Excitation of Decatungstate

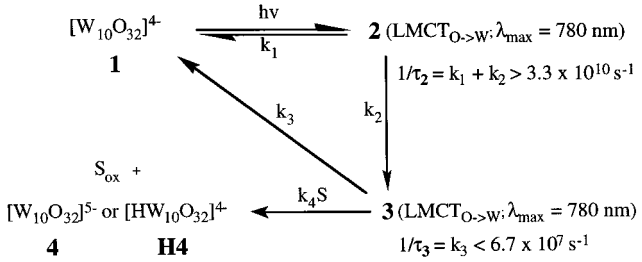

When monitored within 0−15 ns after the picosecond flash excitation of M_4**1** (Na^+ and Q^+ salts exhibited identical transient spectra/behavior on this time scale), an emissive but unreactive transient is produced that was assigned as a ligand-to-metal charge-transfer (LMCT; O → W) excited electronic state **2**.[23] This species has a lifetime (τ) shorter than 30 ps, by both emission[30] and transient absorbance[23] measurements (Scheme 1).[31] A second nonemissive species **3** also was observed by transient absorbance (λ_{max} at 780 nm).[23] This species has a lifetime much longer than 15 ns and a spectrum similar to that of the one-electron reduced product $[W_{10}O_{32}]^{5-}$ (**4**; λ_{max} at 370 and 780 nm).[25,32] However, the absence of an absorption maximum at 370 nm, together with the absence of spectral changes with added reactive quenchers cyclohexene and 2-butanol, demonstrated that the transient **3** must be different from **4**.[23,32] It was proposed that the long-lived intermediate **3** reacted with the quenchers on a time scale >15 ns. This was confirmed by recent reports of the nanosecond transient behavior of photoexcited M_4**1** with the quenchers proprionitrile, adamantane, tetra-*n*-hexylammonium cation, and 2-propanol.[28,29] The reac-

S1089-5639(98)00723-3 CCC: $15.00
Published on Web 05/15/1998

tive intermediate **3** is probably formed directly from **2**, since the quantum yields for the reduction of M_4**1** are independent of excitation wavelength.[19,20]

We report here new evidence from nanosecond flash excitation of M_4**1** in acetonitrile (MeCN) which verifies that **3** is a reactive long-lived intermediate with substantial O → W charge-transfer character and indicates that **3** is a "hot" ground electronic state isomer of M_4**1**. In the presence of a suitable substrate, **3** is converted to **4** or its protonated derivative, **H4**. The rate constants for the reductive quenching of **3** (k_4) by thiocyanate ion or four organic functional groups and the limiting quantum yields for the production of **4** + **H4** measured 0−1 μs after the flash can differentiate electron transfer (et) and hydrogen atom transfer (hat) mechanisms and can determine the fate of the respective geminate pairs.

Experimental Section

Materials. Tetra-*n*-butylammonium (Q^+) and sodium salts of M_4**1** were recrystallized two times from MeCN and were shown by cyclic voltammetry (Bioanalytical Systems; Q^+ salt only) and by FT-infrared (Nicolet 510P) and absorption spectroscopy (Shimadzu 3101/PC) to be free of redox-active impurities.[25,26] The lowest energy band of M_4**1** (λ_{max} = 324 nm) has been assigned previously to an oxygen-to-metal charge-transfer absorption.[33] The ratio of absorbances observed at 262 and 324 nm, A_{262}/A_{324}, for Na_4**1** was 1.14.[34]

Tetra-*n*-butylammonium hexafluorophosphate (Aldrich) was recrystallized five times from ethanol and dried on a high-vacuum line for 4 days. Benzophenone (Aldrich, 99.9+%) and spectroscopic grade MeCN and benzene (Burdick & Jackson) were used as received. Sodium thiocyanate (Baker, 98.1%) was recrystallized two times from water. All other substrates (Aldrich) were of the highest purity available (~99.9%). A control experiment using MeCN predried with activated alumina and distilled from CaH_2 using a high fractionation column (sufficiently pure for electrochemistry) showed transient behavior identical to that of the untreated solvent.

Transient Absorbance Spectrophotometer. Laser excitation was provided from the third harmonic (355 nm) of a Q-switched Nd:YAG laser (Continuum Surelite; 7 ns pulse width; ~7 mm beam diameter). The beam was passed through a half-wave plate/calcite polarizer pair which allowed the beam energy to be varied independently of the flashlamp pump voltage. The latter was set to maximize both the stability and the temporal profile of the pulses output from the harmonic generating crystals. The probe light was obtained from a 150 W Xe arc lamp (Oriel 60001 series housing; arc dimensions, 1.1 mm × 0.5 mm) equipped with a fused-silica collimating lens (50 mm f.l., *f*/1.5). This collimated light was passed though an electromechanical shutter (Vincent Associates, Uniblitz D122/VS25S251), and the arc was imaged with a fused-silica lens (150 mm f.l., *f*/3) onto a variable slit (Oriel) which baffled any emission and was located 4.5 cm beyond the sample cell. The probe and excitation beams overlapped at the sample cell in a 90° arrangement, with slight underfilling of the excitation beam. The probe light was collected and reimaged with a pair of plano-convex fused-silica lenses (150 mm f.l., *f*/3; 125 mm f.l., *f*/2.2) onto a monochromator (PTI, 50 mm × 50 mm grating, 500 nm blaze, 1 mm slit widths) which was equipped with a drive assembly and a photomultiplier tube (PMT; five-stage Hamamatsu R928 operated at −600 V; rise time <1 ns). Schott glass neutral density filters were used to attenuate the probe light as needed, and sharp cutoff filters were used to block second-order grating reflections from reaching the PMT.

The photocurrent was amplified 10-fold and fed into a digitizing oscilloscope (Tektronix 540, 1 GHz sampling rate) which was triggered by a laser sampling fast photodiode. A home-built master oscillator provided timing sequences for the control of the laser flashlamp trigger, Q-switch, probe light shutter, and arc pulser. A PC computer was interfaced to both the oscilloscope and the monochromator drive assembly using the ASYST programming language. Chromatic aberration-induced changes in probe/excitation beam overlap vs probe wavelength were eliminated by either reducing the slit width of the emission baffle or by placing a 5 mm diameter limiting aperture at the front of the sample cell. The 7 ns laser pulse width corresponded to an approximate instrument response time of 21 ns, and the zero time was defined at the point where the instrument response was extinguished. The detector response remained linear up to 1 ms.

Measurements of Transient Absorbance Spectra, Kinetics, and Quantum Yields. A flow cell was used for recording both transient spectra and kinetics measurements with reactive quenchers. This apparatus consisted of a 250 mL three-neck flask as reservoir, a positive displacement Teflon-clad gear pump (Micropump 07002-17, 316 SS head), 4 mm i.d. PTFE Teflon tubing, a 1 cm path length quartz flow cell (Helma), and a filter assembly (Cole-Parmer 06621-05, 1−2 μm porosity; all Teflon-wetted parts). The reservoir was equipped with three adapters: two contained Viton O-rings to accommodate the Teflon tubing, and one contained a Teflon-lined silicone septum for substrate injection and solution deoxygenation. The solutions (150 mL) were purged with MeCN-saturated Ar for at least 1 h prior to flash excitation, and the solutions remained under a stream of Ar during the measurements. The quenchers were degassed with Ar and added to the reservoir via gastight syringes.

All transient absorbance (ΔA) data were collected with 62 μM M_4**1** in MeCN (M = Na^+ or Q^+; 150 mL volume; $A_{355} \sim 0.3$), unless indicated otherwise. Transient absorbance spectra were recorded by averaging 10 laser shots at each wavelength, and kinetic traces were averaged for 15 laser pulses. The kinetic data were each fit between t = 0−800 ns to the function $\Delta A_{\lambda,t} = \Delta A_{\lambda,\infty} + (\Delta A_{\lambda,0} - \Delta A_{\lambda,\infty})e^{-kt}$, which reflects the simultaneous monitoring of reactant decay and product formation at wavelength λ with pseudo-first-order rate constant k. Each quenching rate constant, k_4, was obtained from the slope of a linear Stern−Volmer plot (k vs quencher concentration) using at least seven but usually as many as 15−20 points. Only Na_4**1** was used to obtain k_4 values since Q^+ quenches the initial transient (vide infra). As a check for sample integrity, ground-state absorbance spectra were recorded both before and after each transient absorbance (ΔA) experiment.

When measured at 324 and 780 nm between 0 and 1 μs, the transient absorbances derived from excitation of either Na_4**1** or Q_4**1** remain linear with laser excitation energy over the 0−10 mJ/pulse range (see Supporting Information).[35] All transient measurements were recorded within this linear region. Quantum yields for the transients were obtained by triplet benzophenone actinometry (eq 1)

$$\frac{\Phi_x \Delta\epsilon_x}{\Phi_{^3BP} \Delta\epsilon_{^3BP}} = \frac{\lim_{E\to 0}\left(\frac{d(\Delta A_x)}{dE}\right)(1 - 10^{-A})_{\lambda,^3BP}}{\lim_{E\to 0}\left(\frac{d(\Delta A_{^3BP})}{dE}\right)(1 - 10^{-A})_{\lambda,x}} \qquad (1)$$

where x denotes the species of interest, ^{3}BP is the benzophenone triplet, $\Delta\epsilon$ and ΔA are the changes in molar absorptivity and absorbance relative to the ground state, respectively, A_λ is the

ground-state absorbance at the irradiating wavelength λ, and E is the incident laser energy.[36] The initial slopes obtained from plots of ΔA vs incident laser energy combined with the literature reference values, $\Phi_{3BP} = 1.00$ and $\Delta\epsilon_{530} = 7220\ M^{-1}\ cm^{-1}$, allow access to the product, $\Phi_x\Delta\epsilon_x$. Following excitation of either Q_4**1** or Na_4**1**, the transient measured at $t = 0$ ns (identified below as the reactive intermediate **3**) gives $\Phi_3\Delta\epsilon_3 = 3440 \pm 100\ M^{-1}\ cm^{-1}$ at 780 nm.

The quantum yields of the one-electron reduced decatungstate products, Φ_{4+H4}, were obtained at different substrate concentrations by measuring $\Delta A(t)$ at 780 nm using **3** as an internal actinometer. The incident laser energy was maintained within the region where $d(\Delta A)/dE$ is constant and the ground-state absorbances at the excitation wavelength (355 nm) were identical ($A_{355} \sim 0.3$) to that used in determining the product $\Phi_3\Delta\epsilon_3$ described above. Under these conditions eq 1 simplifies to eq 2,

$$\Phi_{4+H4} = \frac{\Delta A_{4+H4}}{\Delta A_3}\frac{\Phi_3\Delta\epsilon_3}{\Delta\epsilon_{4+H4}} \qquad (2)$$

where at 780 nm $\epsilon_{H4} \sim \epsilon_4 = 7000 \pm 100\ M^{-1}\ cm^{-1}$.[25,26] Consequently, the quantum yields for the reduced products **4** + **H4** are accessible without prior knowledge of either the extinction coefficient or the quantum efficiency for the formation of the intermediate **3**, although evidence exists that Φ_3 is 0.50.[20] Assuming that Φ_3 is 0.50, then from the measured value for $\Phi_3\Delta\epsilon_3$ of 3440 ± 100, ϵ_3 is 6880 ± 240, which is identical within experimental error to ϵ_4 and ϵ_{H4}. Estimating the cell path length to be 0.7 cm (laser beam diameter) and taking ϵ_3 to be 6880 $M^{-1}\ cm^{-1}$, the ΔA at saturation[35] gives $\Phi_3 \sim 0.5$. Since nearly all the measurements reported here reflect initial transient absorbances of 0.07 at 780 nm, the initial concentration of **3** is 14 μM, corresponding to 23% conversion of M_4**1** to **3** and an overall 46% bleaching of M_4**1**.

Results

A. Photoexcitation of $M_4$1 (M = Na^+ or Q^+) in MeCN: Assignments of Transient Spectra and "Background" Reactions. The 355 nm laser excitation (9 mJ energy, 7 ns pulse width) of M_4**1** in MeCN produces small quantities of the one-electron reduced product $[W_{10}O_{32}]^{5-}$ **4** and/or its protonated derivative **H4** by oxidation of Q^+ or MeCN.[37] Excitation of either salt proceeds through the same initial transient (Figure 1, top; $t = 0$ ns), and both transients undergo first-order decay (Figure 2; τ in Table 1)[38] to products that are identical except for ~3 times greater intensity with M = Q^+.

The initial transient spectrum ($t = 0$ ns) matches one observed 0.1−15 ns after picosecond excitation (λ range: 390−860 nm) which had been earlier assigned to a reactive intermediate **3** (Scheme 1).[23] The wider spectral range monitored here precludes its assignment to **4** because of the absence of an absorption maximum at 375 nm (Figure 1, top). Therefore, intermolecular photoinduced charge transfer within a {M_4**1**- - substrate} ground-state adduct is not important as has been earlier concluded by others.[22,32] However, the product of the initial transient decay does exhibit a spectrum nearly identical to **4** (Figure 1, bottom), although the intensity of the 375 nm band relative to 780 nm is smaller than expected, probably because of complete or partial protonation of **4** to **H4** (vide infra).

The initial transient must therefore be a reactive intermediate **3**, since both its lifetime is shortened and the **4** + **H4** yield is increased ~3 times when Q^+ is present (Table 1), in accord with steady-state quantum yield (Φ) measurements.[32,37] Furthermore, its kinetic behavior with added substrates substantiates this assignment (vide infra). These results and conclusions are in agreement with those reported in recent similar studies.[28,29,39] The marginal quenching of **3** by MeCN still allows for lifetime

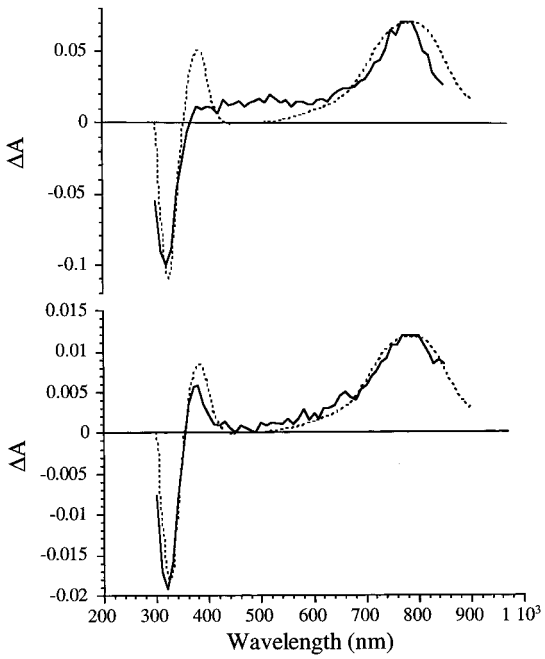

Figure 1. Transient absorbance (ΔA) spectra at $t = 0$ ns (top solid line) and $t = 800$ ns (bottom solid line) following 355 nm laser pulsed excitation (~9 mJ) of 62 μM Q_4**1** in MeCN. Calculated ΔA spectra of **4** (the one-electron reduction product of Q_4**1**) normalized at 780 nm (dotted line) are shown for comparison.

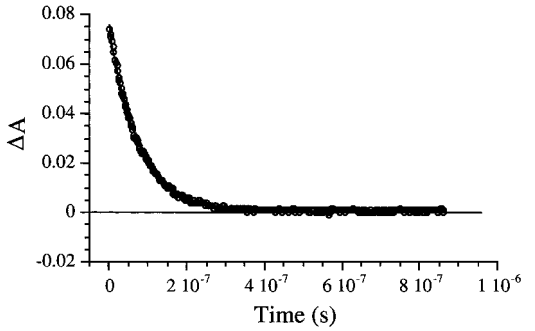

Figure 2. Transient absorbance (ΔA) decay kinetics observed at 780 nm following the 355 nm pulsed excitation (~9 mJ) of 62 μM Na_4**1** in MeCN-d_3. Single-exponential fit results: $\Delta A(\infty) = 0.0006$; $\Delta A(0) = 0.0771$, $\tau = 73.6 \pm 0.03$ ns; $R^2 = 0.998$.

TABLE 1: Lifetime Quenching of 3 by MeCN, MeCN-d_3, and the Q^+ Counterion[a]

M_4**1**	τ_3 (±1 ns)[b]	ΔA_3 (±0.002)[c]	ΔA_{4+H4} (±0.0005)[d]	Φ_{4+H4}[e]
M = Q^+	56	0.073	0.0132	0.089 ± 0.005[f]
M = Na^+	68	0.071	0.0047	0.032 ± 0.004[f]
M = Na^+ [g]	36	0.073	0.0320	0.215 ± 0.010
M = Na^+ [h]	74	0.072	0.0006	0.004 ± 0.003

[a] Observed by transient absorbance (ΔA) at 780 nm following 355 nm laser pulsed excitation (~9 mJ) of 62 μM M_4**1** in MeCN with $OD_{355} \sim 0.3$; Q^+ = tetra-*n*-butylammonium. [b] Lifetime of single-exponential decay. [c] Maximum absorbance at $t = 0$ ns. [d] Asymptote from the single-exponential decay fit between $t = 0$−800 ns. [e] From eq 2. [f] Average of six independent measurements yields $\Phi_{4+H4} = 0.087 \pm 0.002$ for Q_4**1** and $\Phi_{4+H4} = 0.033 \pm 0.002$ for Na_4**1**. [g] Added 6 mM $Q[PF_6]$. [h] In MeCN-d_3.

TABLE 2: Bimolecular Quenching Rate Constants and Geminate Pair Yields

substrate[a]	$k_4 \times 10^{-7}$ (M^{-1} s^{-1})[b] (±5%)	$\Phi_{\mathbf{H4},\mathrm{lim}}$[c] (± 0.02)
DMA	720	
DEA	620	
DMPT	790	
thianthrene	229	
sodium thiocyanate	19.7	≥0.09[d]
±2-butanol	9.93	0.50 (0.49)
cyclopentane	2.39	0.50 (0.35)
h_{12}−cyclohexane	3.25	0.46 (0.44)
d_{12}−cyclohexane	1.09	0.44 (0.24)
cycloheptane	5.59	0.48 (0.45)
cyclooctane	7.79	0.47 (0.46)
DMC	4.27	0.50 (0.49)
cis-decalin	8.53	0.48 (0.40)

[a] DMA, DEA, DMPT, and DMC are *N*,*N*-dimethylaniline, *N*,*N*-diethylaniline, *N*,*N*-dimethyl-*p*-toluidine, and *cis*-1,2-dimethylcyclohexane, respectively. [b] See Scheme 2 for definition. [c] Limiting quantum yields $\Phi_{\mathbf{H4},\mathrm{lim}}$, corrected for MeCN quenching, were determined from unweighted nonlinear least-squares fits of experimental Φ^{-1} vs $[Q]^{-1}$ curves to eq 8. The uncorrected values, $\Phi_{\mathbf{H4},\mathrm{app-lim}}$, obtained from fits to "linear" portions of the curves, are in parentheses. [d] Quantum yield for **4** obtained at the limit of Na[SCN] solubility in MeCN, 0.9 M.

quenching and quantum yield measurements with other added substrates with Na_4**1** giving less interference than Q_4**1**. The rate constant for the intrinsic decay of **3**, k_3, must be less than or equal to 1.35×10^7 s^{-1} as is measured under the least reactive conditions, i.e., Na_4**1** in MeCN-d_3 (Table 1).

The lifetimes of **3** (although different for M = Q^+ or Na^+) remain unaffected by the concentration of M_4**1** (5−500 μM), by the excitation energy (2−40 mJ/pulse), by the concentration of H_2O in the range from 0 to 5 mM, and by concentrations of oxygen produced by 1 atm pressure. Furthermore, $\Phi_{\mathbf{4+H4}}$ remains constant over the 0−40 mJ/pulse range of excitation energies. These results indicate that self-quenching of **3** is unimportant and that neither H_2O nor O_2 quenches **3** appreciably or affects the yield of **4** + **H4** over the 0−1 μs time range.[40] The small quantities of **4** + **H4** generated by flash excitation of M_4**1** decay by a second-order process with rate constants $k = (1.8 \pm 0.2) \times 10^8$ M^{-1} s^{-1} (M = Na^+ in MeCN; $[\mathbf{4} + \mathbf{H4}]_0 = 0.96$ μM) and $k \sim 1 \times 10^9$ M^{-1} s^{-1} (M = Q^+ in MeCN; $[\mathbf{4} + \mathbf{H4}]_0 = 2.69$ μM).[41]

B. Quenching of 3 by Thiocyanate, Thianthrene, and Aromatic Amines. Rate constants for the dynamic quenching of **3** (derived from Na_4**1**) by these substrates were obtained from the slopes of linear Stern−Volmer plots (see Supporting Information) and are collected in Table 2. *N*,*N*-Dimethylaniline (DMA), *N*,*N*-diethylaniline (DEA), and *N*,*N*-dimethyl-*p*-toluidine (DMPT) all quench **3** at diffusion-controlled rates ($k_4 = (6-8) \times 10^9$ M^{-1} s^{-1}) but produce no net reduction product **4** + **H4**. Thianthrene and sodium thiocyanate exhibit somewhat smaller quenching rate constants of $(2.3 \pm 0.1) \times 10^9$ and $(2.0 \pm 0.1) \times 10^8$ M^{-1} s^{-1}, respectively, with the latter producing appreciable quantities of **4** + **H4**.

Even though the lifetime of **3** is quenched more than 90% by thianthrene or the amines, no reduction products are detected since the transient absorbance decays to zero at all wavelengths (Supporting Information).[42] Similar behavior is observed for thiocyanate at concentrations lower than 0.2 M, where the quenching of **3** is ∼80% complete. However, at higher concentrations of thiocyanate, both **4** and $[(SCN)_2]^{\bullet-}$ (λ_{max} = 475 nm)[43,44] are detected, and their yields both continue to increase as the thiocyanate concentration is raised further (Figure 3).[45]

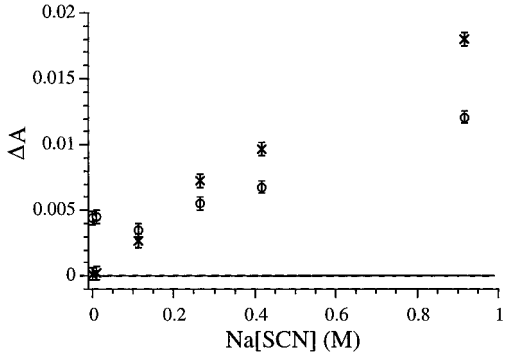

Figure 3. Transient absorbance (ΔA) decay asymptotes measured between 200 and 800 ns (○, λ_{obs} = 780 nm assigned to **4**; ×, λ_{obs} = 475 nm assigned to $[(SCN)_2]^{\bullet-}$) vs thiocyanate concentration following pulsed excitation of 62 μM Na_4**1** in MeCN.

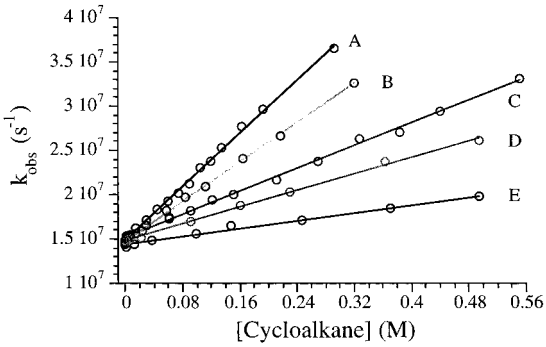

Figure 4. Stern−Volmer plots for the lifetime quenching of **3** by cycloalkanes. The lifetimes of **3** were measured by transient absorbance (ΔA) at 780 nm following 355 nm pulsed excitation (∼9 mJ) of 62 μM Na_4**1** in MeCN with different concentrations of the following cycloalkanes: A, cyclooctane; B, cycloheptane; C, cyclohexane-h_{12}; D, cyclopentane; E, cyclohexane-d_{12}.

C. Quenching of 3 by Cycloalkanes and 2-Butanol. Stern−Volmer plots for the quenching of **3** (derived from Na_4**1**) by a series of cycloalkane substrates (Figure 4) yield quenching rate constants between 10^7 and 10^8 M^{-1} s^{-1} that increase with the ring size of the cycloalkane (Table 2). A primary kinetic isotope effect is observed for quenching by cyclohexane-h_{12}/cyclohexane-d_{12} ($k_{4,h}/k_{4,d}$ = 3.0).

As the lifetime of **3** is quenched, an increase in the absorbance asymptote at 780 nm is observed, indicating formation of **4** + **H4** (see Supporting Information). The observed quantum yields $\Phi_{\mathbf{4+H4}}$ approach saturation at high substrate concentrations (Figure 5) and **4** + **H4** does not decay appreciably up to 1 ms after excitation (see Supporting Information).

Discussion

Redox Properties of $M_4$1, 3, 4, and H4. The LMCT absorbance band edge of M_4**1** in MeCN near 420 nm places an upper limit of 2.95 ± 0.05 eV (68.0 kcal/mol) on the internal energy of **3**. In MeCN, Q_4**1** exhibits two reversible one-electron waves with formal potentials of −1.20 and −1.80 V vs Ag/$AgNO_3$.[20,26] Assuming negligible differences in entropy between Q_4**1** and **3**, the potential of the one-electron redox couple **3**/**4** is estimated to be ≤1.75 V vs Ag/$AgNO_3$ (≤2.23 V vs NHE), and driving forces for electron transfer are listed in Table 3. In strongly acidic MeCN, the two reversible one-electron waves of Q_4**1** collapse to a single quasi-reversible two-electron wave at −0.10 V vs Ag/$AgNO_3$,[20] showing that protonation results in a substantial anodic shift. This effect influences final product distributions and product quantum yields.[18,20]

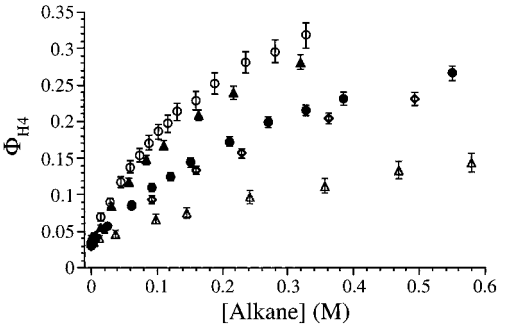

Figure 5. Dependence of the quantum yield for the formation of **H4** (measured from the asymptote of the transient absorbance decay at 780 nm) on initial cycloalkane concentration following the 355 nm pulsed excitation (~9 mJ) of 62 μM Na_4**1** in MeCN: cyclooctane (○); cycloheptane (▲); cyclohexane-h_{12} (●); cyclopentane (◇); cyclohexane-d_{12} (△). Without cycloalkane, the nonzero Φ_{H4} derives from quenching by MeCN.

TABLE 3: Free Energies for Electron-Transfer Quenching of 3 and Thermal Back Electron Transfer[a]

substrate	oxidation potential[b] (V vs NHE)	$\Delta G^{\circ\prime}_{et}$ (±0.06 eV) forward[c,d]	forward[c,e]	back[f]
DMPT	0.94	−1.63	0.018	−1.32
DEA	0.99	−1.58	0.068	−1.37
DMA	1.04	−1.53	0.12	−1.42
thianthrene	1.62	−0.95	0.70	−2.00
NaSCN	1.60	−0.90	0.75	−2.05

[a] All free energies are corrected for the Coulombic work term, $(Z_{1a}Z_{2a} - Z_{1b}Z_{2b})(e^2f/Dr_{12})$, where Z_{xy} is the charge of species x in geminate pair y, and the e^2f/Dr_{12} term is taken as 0.068 eV ($f = 1$, $D = 35$, $r_{12} = 6$ Å). [b] Reported from measurements in MeCN vs SCE[57,58] and referenced here vs NHE using NHE vs SCE = +0.23 V. [c] Forward electron transfer: $\mathbf{3} + S^n \rightarrow \mathbf{4} + S^{(n+1)}$ where S denotes substrate of charge n. [d] Assumes +2.23 V vs NHE for the reduction potential of **3** (based on the 420 nm LMCT band edge in M_4**1**, see text). [e] Assumes +0.58 V vs NHE for the reduction potential of **3** (based on a shortest emission wavelength for **3** of 950 nm, see text). [f] Thermal back electron-transfer calculated from −0.72 V vs NHE as the oxidation potential of **4**.[19,26]

Electronic Structure of 3. In less than 30 ps, **3** is formed via the unreactive LMCT intermediate **2** (Scheme 1).[23,30,38] In both **4** and its two-electron reduced derivative $[W_{10}O_{32}]^{6-}$, the added electrons are located primarily among the eight equatorial tungsten ions.[26,46] Because **3** and **4** have similar visible spectra, **3** probably also has significant electron density on the equatorial tungstens, and therefore, much of the O → W charge-transfer character of **2** is retained in **3**. Consequently, the differences in the UV spectra of **3** and **4** likely derive from the presence in **3** of one or more electron-deficient oxygens that are absent in **4**.[23]

The factors that govern the lifetimes and emission of polyoxometalate excited states in solution have not been addressed.[47,48] In general, polyoxometalates in solution emit either very weakly with subnanosecond lifetimes or not at all.[7,30] Nevertheless, three key observations form a basis for assignment of the electronic structure in **3**. First, as described above, **3** has O → W charge-transfer character. Second, as measured in MeCN-d_3, the intrinsic decay rate of **3** must be less than or equal to 1.35×10^7 s^{-1}. Third, no laser-induced emission from **3** is detected (quantum yield detection limit ~10^{-4}) between 300 and 900 nm, which restricts the radiative rate constant to less than 1.35×10^3 s^{-1}.

It is difficult to rationalize such a low radiative rate constant unless the electric dipole transition **3** → M_4**1** is both spin- and parity-forbidden. However, the spin restriction should be relaxed by the significant spin−orbit coupling of tungsten, making assignment of **3** to an excited state unlikely. Although our observations do not preclude possible emission at $\lambda > 900$ nm, such a low internal energy would render **3** unreactive, i.e. implying a reduction potential of ≤+0.58 V vs NHE assuming an emission onset at $\lambda = 950$ nm (Table 3). More likely, **3** may be a "hot" ground-state isomer of M_4**1**, residing in an energy minimum considerably distorted relative to M_4**1** (Figure 6A). Such a large distortion would produce significant localization of the separated charges, and the lifetime of **3** would be governed by the height and shape of the barrier between the minima for **3** and M_4**1**. This model reconciles the lack of detectable emission without imposing an unusually small radiative rate constant and allows for the storage of considerable light-induced chemical potential.

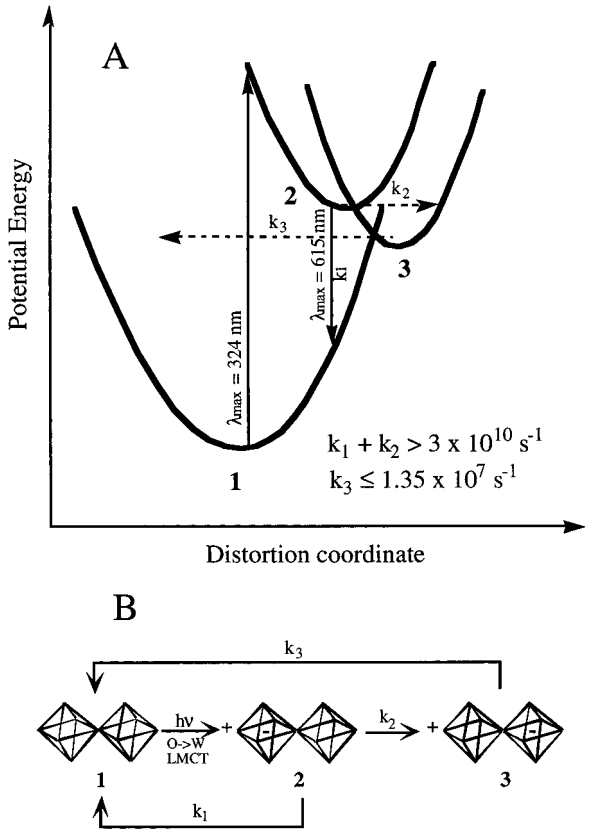

Figure 6. "Hot" ground-state model for the electronic structure of **3**. (A) Schematic representation of potential energy vs distortion coordinate for M_4**1**, **2**, and **3**. The avoided crossing between the surfaces of **3** and **1** is omitted for clarity. (B) Plausible model for the observed long lifetime of **3**. Each octahedron represents one W atom surrounded by six O atoms. Only two of the 10 WO_6 octahedra are shown, and the light-induced separated charges are shown as + and −.

A plausible explanation for the long lifetime of **3** is illustrated in Figure 6B. The unreactive LMCT (O → W) excited state **2**[23] presumably has charge separation localized within a single WO_6 octahedron. From **2**, rapid relaxation to **3** ensues, with concomitant transfer of electron density to a tungsten on an adjacent octahedron, producing further charge separation. A similar model has been advanced by Kraut and Ferraudi for the reactive intermediate produced by photoexcitation of α-$[Mo_7O_{24}]$.[6−8]

Evidence exists that the electronic structure of **4** is class II mixed valence,[25,49] that the d electron is localized on one or perhaps two equatorial WO_6 octahedra,[25] and that the hopping of the d electron between equatorial tungsten sites requires less than 1 ns.[25,46] Since the electrostatic attraction of the separated

SCHEME 2: Kinetic Model for the Photochemistry of Decatungstate

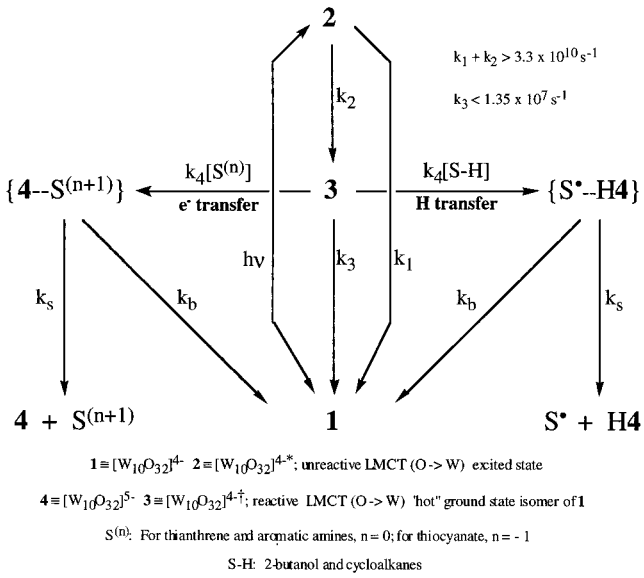

charges in **3** should lead to an even shorter residence lifetime, the measured long intrinsic lifetime of **3** ($\tau > 74$ ns) would require larger nuclear distortions accompanying charge separation in **3** than those which accompany electron hopping between tungstens in **4**. Such an enhanced distortion in **3** would derive from significant localization of positive charge on an oxygen site in **3** which is absent in **4**. Without evidence for a long-lived emission from **3** in the visible region, a "hot" ground state with O → W charge transfer character is a likely assignment for **3**.

Decatungstate Photochemistry. A. Reaction Mechanisms for the Early Events. To date, no direct evidence is available for electron transfer to a photoinduced polyoxometalate intermediate. However, the observation of both **4** and $[(SCN)_2]^{\bullet-}$ at high thiocyanate quencher concentration demonstrates electron-transfer quenching of **3** by thiocyanate to form the geminate pair {**4**- -SCN•}, which can either undergo back electron transfer or SCN• can be scavenged by additional SCN^-.[44] For the following reasons, the same is likely true for thianthrene and the amines, even though the expected radical ion intermediates are not observed in our flash experiments. First, back electron transfer could be too fast to allow for a detectable concentration of the geminate radical ion pair on the nanosecond time scale. Second, these substrates possess low oxidation potentials such that electron transfer is energetically feasible (Table 3). Third, energy-transfer quenching is obviated by the absence of states able to accept the ≤2.95 eV internal energy of **3**. Fourth, as described above, **3** likely has substantial charge-transfer character. Finally, thermal reactions between polyoxometalates and electron-rich substrates are dominated by electron transfer.[1−4,50]

In contrast, both quantum chemical calculations and a large body of indirect experimental evidence, including product distributions, initial-rate kinetics data, and thermodynamic considerations, support a hydrogen atom abstraction mechanism for the photodehydrogenation of saturated hydrocarbons and alcohols by M_4**1**.[19,20,51] Furthermore, the primary kinetic isotope effect for the quenching of **3** by cyclohexane-h_{12}/cyclohexane-d_{12} ($k_{4,h}/k_{4,d} = 3.0$) provides direct evidence for a transition state involving substantial C−H cleavage.[52]

Scheme 2 illustrates a kinetic model that retains the minimum features necessary to describe the early events in the oxidation of substrates by intermediate **3**, where k_3 is the rate constant for the intrinsic decay of **3**, k_4 is the rate constant for substrate-induced quenching of **3**, k_s and k_b are the rate constants for the separation and back-reaction of the geminate product pairs, S and SH represent electron-transfer and hydrogen atom-transfer quenchers, respectively, and {**4**- -S•+} and {**H4**- -S•} represent the geminate pairs which are considered to be either solvent-separated or associated complexes, i.e., radical/radical ion intermediates bound to the oxide surface of reduced decatungstate. The fates of these geminate pairs partition between two competing processes: a back-reaction that regenerates M_4**1** and either S or SH and a separation into freely diffusing intermediates, either **4** and the radical cation S•+ or **H4** and the radical S•. This model predicts biexponential behavior when $k_b + k_s \sim k_3 + k_4[Q]$, where Q represents either S or SH.

The theoretical quantum yield for the formation of **4** or **H4** is expressed by eq 3, where ϕ_3 is the quantum efficiency for forming **3**, and Q represents the operative quencher. If $k_4[Q] \gg k_3$, eq 3 is reduced to an expression for the limiting quantum yield, eq 4, which

$$\Phi_{\mathbf{4}\text{ or }\mathbf{H4}} = \phi_{\mathbf{3}}\left(\frac{k_4[Q]}{k_3 + k_4[Q]}\right)\left(\frac{k_s}{k_b + k_s}\right) \tag{3}$$

$$\Phi_{\mathbf{4}\text{ or }\mathbf{H4},\mathrm{lim}} = \phi_{\mathbf{3}}\left(\frac{k_s}{k_b + k_s}\right) \tag{4}$$

is bounded by two conditions: $\Phi_{(\mathbf{4}\text{ or }\mathbf{H4}),\mathrm{lim}} \sim 0$ when $k_b \gg k_s$ and $\Phi_{(\mathbf{4}\text{ or }\mathbf{H4}),\mathrm{lim}} \sim \phi_{\mathbf{3}}$ when $k_b \ll k_s$.

B. Electron-Transfer Quenching. The quenching rate constants k_4 for the amines (Table 2) do not reflect differences in their oxidation potentials (Table 3) because the reactions are diffusion-controlled and the driving forces are too exergonic. However, for thianthrene and thiocyanate, lower exergonicities do lead to slower quenching rate constants, as is consistent with an electron-transfer mechanism.[53]

The decay of **3** remains first-order for all concentrations of added thiocyanate, thianthrene, or amine. Therefore, $k_b + k_s \gg k_3 + k_4[Q]$ or $k_b + k_s \ll k_3 + k_4[Q]$. The lack of observable products within the $\Delta A \sim 5 \times 10^{-4}$ detection limit (excluding thiocyanate at concentrations greater than 0.2 M) indicates, however, that $k_b + k_s \gg k_3 + k_4[Q]$ and, from eq 3, that $k_b \geq 43k_s$.[54] Consequently, product accumulation is negated by a rapid back electron transfer that occurs prior to separation of the geminate pair.

This is not surprising for two reasons. First, except with the geminate pair {**4**- -SCN•}, a substantial electrostatic attraction (∼0.34 ± 0.03 eV) must be overcome in order for the ion pairs to separate. Second, the back electron transfer is highly exergonic (Table 3). Since the forward electron-transfer rate is diffusion-controlled, the back electron-transfer rate must also be very fast, assuming similar reorganization energies and normal Marcus behavior for both transfers.

For thiocyanate, the situation is different. The absence of electrostatic attraction in {**4**- -SCN•} increases k_s compared with that in an ion pair. Furthermore, despite the exceedingly exergonic back electron transfer (−2.05 eV), the observation of $[(SCN)_2]^{\bullet-}$ at thiocyanate concentrations greater than 0.2 M demonstrates that capture of thiocyanogen radical by thiocyanate can be competitive with k_b. Modifying Scheme 2 to account for this additional decay pathway for the geminate pair {**4**- -SCN•}, the reciprocal quantum yield expression for the formation of **4** in the presence of SCN^- is shown in eq 5,

$$\frac{1}{\Phi_4} = \frac{1}{\phi_3}\left\{1 + \left(\frac{k_s + k_b}{k_i} + \frac{k_3}{k_4}\right)\frac{1}{[SCN^-]} + \left(\frac{k_3(k_s + k_b)}{k_i}\right)\frac{1}{[SCN^-]^2}\right\} \quad (5)$$

where k_i is the rate constant for the scavenging of $SCN^\bullet$ by SCN^- within the geminate pair. Unfortunately, the small Φ_4 values obtained within the solubility limit of NaSCN in MeCN preclude modeling this expression to obtain $k_i/(k_s + k_b)$. Furthermore, dependencies of ionic strength on the rate constants in eq 5 may be expected as the NaSCN concentration is increased. Nevertheless, substituting $\Phi_4 = 0.09$ observed at 0.9 M NaSCN into eq 5 indicates that $k_i/(k_s + k_b) \sim 0.26$. Assuming that $k_i \sim 2 \times 10^9\ M^{-1}\ s^{-1}$, i.e., diffusion-controlled, then $k_s + k_b \sim 8 \times 10^9\ s^{-1}$, and since $k_b \geq 43k_s$ then $k_b \sim \geq 8 \times 10^9\ s^{-1}$.

Thus, the net oxidation of neutral substrates by electron transfer to **3** has a low quantum yield because of slow ion-pair separation (electrostatically unfavorable) and rapid back electron transfer. However, product yields can be improved if the pair reacts with a chemical scavenger, e.g., SCN^-, or if **4** becomes protonated at rates competitive with the back-reaction. Protonation of **4**, resulting from either an external proton source or deprotonation of the cation radical within the geminate pair, decreases the exergonicity[20] and therefore reduces the rate of the back-reaction.

C. Hydrogen Atom Transfer Quenching. 1. "Background" Quenching of 3 by MeCN. Determining the kinetic isotope effect for quenching of **3** by MeCN and MeCN-d_3 is not possible without information on k_3, the intrinsic lifetime of **3** which is not accessible because of interfering solvent quenching.[37] Even so, the different lifetimes and quantum yields observed in MeCN vs MeCN-d_3 place a limiting value on k_3 and, for the oxidation of MeCN, place limiting values on k_4 and $k_s/(k_s + k_b)$. These differences are reflected in eqs 6 and 7

$$\frac{\tau_{MeCN-d_3}}{\tau_{MeCN}} = \frac{k_3 + k_{4,MeCN}[MeCN]}{k_3 + k_{4,MeCN-d_3}[MeCN\text{-}d_3]} \quad (6)$$

$$\left(\frac{\Phi_{D4}}{\tau}\right)_{MeCN-d_3}\left(\frac{\tau}{\Phi_{H4}}\right)_{MeCn} = \left(\frac{k_s + k_b}{k_4}\right)_{MeCN-d_3}\left(\frac{k_4}{k_s + k_b}\right)_{MeCN} \geq 10 \pm 1 \quad (7)$$

where τ is the experimentally determined lifetime of **3**, and the equivalence of $k_{s,MeCN}$ and $k_{s,MeCN-d3}$ is assumed. Assuming further that $k_3 \gg k_{4,MeCN-d3}[MeCN\text{-}d_3]$, eqs 3 and 6 give following limiting values: $k_3 \leq (1.35 \pm 0.01) \times 10^7\ s^{-1}$, $k_{4,MeCN} \geq (6.00 \pm 1.49) \times 10^4\ M^{-1}\ s^{-1}$, and $(k_s/(k_s + k_b))_{MeCN} \leq 0.842 \pm 0.087$. The size of the inequality in eq 7 indicates a substantial primary isotope effect in k_4 with considerable C−H cleavage from MeCN in the transition state, although its magnitude may be reduced by an inverse isotope effect anticipated for back electron transfer, k_b, within the geminate pair {**H4**- -$^\bullet CH_2CN$}. The rate constants for the decay of **4** + **H4** from oxidation of Q^+ and for the decay of **H4** from oxidation of MeCN are consistent with back electron transfer to the respective oxidized intermediates.

2. Formation of Geminate Radical Pairs. The observation of a primary kinetic isotope effect $k_{4,h}/k_{4-d} = 3.0$ for the bimolecular quenching of **3** by cyclohexane-$(h/d)_{12}$ indicates substantial C−H cleavage in the transition state consistent with the geminate pair {**H4**- -cyclohexyl radical}, either as a solvent-separated pair or with the radical associated to the oxide surface of **H4**. The quenching rate constants within the series of cycloalkanes do not differ greatly and are similar to that for 2-butanol (Table 2). This is surprising for two reasons. First, unactivated hydrocarbon C−H bonds are usually much less reactive than the C−H bonds of alcohols.[55] Second, the large differences in "instantaneous" quantum yields, i.e., extrapolated to $t = 0$, for substrate oxidation reported under continuous irradiation[20] (Table 4) cannot derive from differences in quenching rate constants alone, but must reflect subsequent steps that may include a back electron transfer within the geminate pair, disproportionation/combination of the radicals,[19,20,56] and/or oxidation of the alkyl radicals by M_4**1** (only likely for the more reducing α-hydroxycarbinyl radical).[55,56]

TABLE 4: Product Quantum Yields for Substrate Photooxidation by 3

substrate[a]	product yield (%)[b,c] alkene, dimer, ketone	Φ (overall)[b,d]	Φ_{H4} (geminate)[e]
cyclooctane	57, 43, 0	0.16	0.34
cyclohexane	25, 32, 37	0.02	0.25
cis-1,2-dmc[f]	45, 0, 0 (50% trans-isomer)	0.04	0.28
cis-decalin	0, 0, 0 (100% trans-isomer)	0	0.36

[a] 0.48 M. [b] Data taken from refs 15, 17, and 18. [c] Percentages of alkane-derived products divided by total products. [d] Measured from the initial rates of the continuous illumination of 3.35 mM Q_4**1** (optically dense) at 322 nm in MeCN by ferrioxolate actinometry.[15,17,18] [e] Calculated for 0.48 M substrate concentration using eq 3 and the $k_s/(k_s + k_b)$ values obtained from fitting plots of Φ_{H4}^{-1} vs [substrate]$^{-1}$ to eq 8 by nonlinear least squares (Figure 7). [f] *cis*-1,2-Dimethylcyclohexane.

3. Limiting Quantum Yields of the Geminate Radical Pairs: Back-Reaction vs *Pair Separation.* The partitioning of the decay of the geminate radical pairs between an irreversible back-reaction (k_b) and a reversible solvent cage escape (k_s) can be determined, in principle, from double-reciprocal plots of the quantum yield vs quencher concentration, where the intercept is the reciprocal of the limiting quantum yield, eqs 3 and 4. However, for 2-butanol and the cycloalkanes, plots of Φ_{H4}^{-1} vs $[Q]^{-1}$ proved to be curved, particularly at lower quencher concentrations where the relative contribution to the formation of **H4** from MeCN oxidation is important (Figure 7). Modifying the quantum yield expression in eq 3 to account for MeCN oxidation leads to eq 8,

$$\frac{1}{\Phi_{H4}} = \frac{1}{\phi_3}\left(\frac{k_3 + k_{4,MeCN}[MeCN] + k_4[Q]}{\left(\frac{k_{s,MeCN}}{k_{b,MeCN} + k_{s,MeCN}}\right)k_{4,MeCN}[MeCN] + \left(\frac{k_s}{k_b + k_s}\right)k_4[Q]}\right) \quad (8)$$

which predicts significant deviation from linearity in plots of Φ_{H4}^{-1} vs $[Q]^{-1}$ at low substrate concentrations. Linearity eventually can be attained only when $(k_s k_4[MeCN]/(k_s + k_b))_{MeCN} \ll (k_s k_4[Q]/(k_s + k_b))_Q$ and when $k_3 + k_{4,MeCN}[MeCN] \ll k_4[Q]$. The linearity observed over a wide range of high quencher concentrations indicates that the apparent limiting quantum yield $\Phi_{H4,app-lim}$ approaches the real limiting yield $\Phi_{H4,lim}$ as is true for 2-butanol (see Supporting Information), but quenchers with poor solubilities and small quenching rate constants are problematic. Of the quenchers examined here, cyclopentane and deuterated cyclohexane represent the worst cases, where "linear" fits to three points at the highest alkane

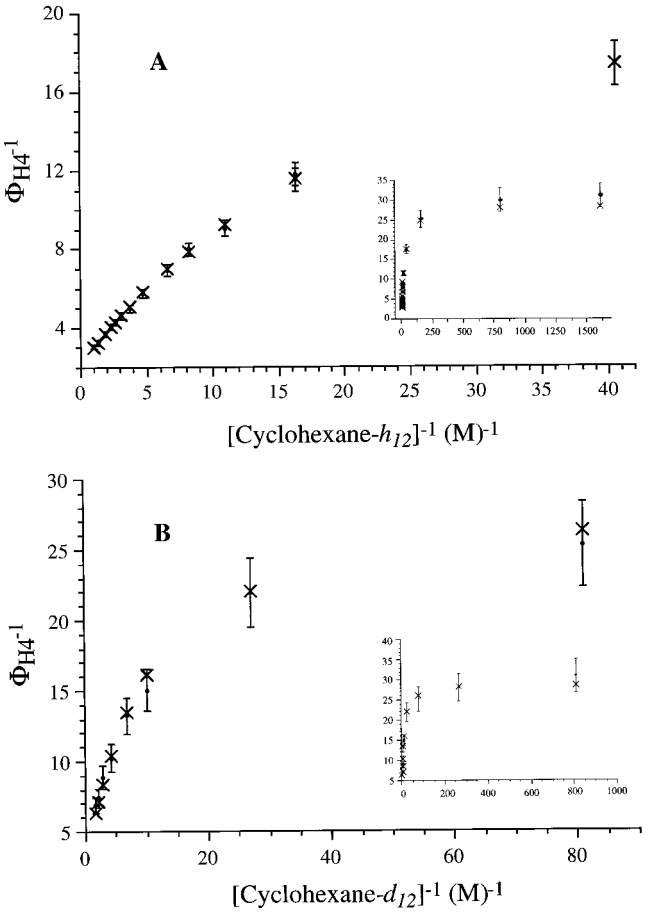

Figure 7. Dependence of reciprocal **H4** quantum yield on reciprocal quencher concentration: (A) cyclohexane-h_{12}; (B) cyclohexane-d_{12}. Error bars on the data (●) are one standard deviation. The curves were fit (×) to eq 8 in order to account for the $\Phi_{\mathbf{H4}}$ contribution from MeCN oxidation.

concentrations lead to $\Phi_{\mathbf{H4},\text{app-lim}} = 0.35$ and 0.26 ± 0.02, respectively. Although their difference from the theoretical maximum ($\phi_{\mathbf{3}} \sim 0.5$) can be rationalized via differences in k_b and k_s (e.g., an inverted isotope effect in k_b could explain the low value of $\Phi_{\mathbf{H4},\text{app-lim}}$ for C_6D_{12} relative to C_6H_{12}, Table 2), correcting for MeCN quenching is warranted.

The corrected limiting quantum yields $\Phi_{\mathbf{H4},\text{lim}}$ were obtained by unweighted nonlinear least-squares fitting of the experimental $\Phi_{\mathbf{H4}}^{-1}$ vs $[Q]^{-1}$ curves to eq 8. Cyclohexane was chosen as a reference to model the curvature of the $\Phi_{\mathbf{H4}}^{-1}$ vs $[Q]^{-1}$ plots derived from MeCN oxidation since its data set contained the greatest point density in the curved region and a well-developed "linear" region apparent at high cyclohexane concentration (Figure 7, top). The experimental $\Phi_{\mathbf{H4}}^{-1}$ vs $[Q]^{-1}$ curve was fit for the adjustable parameters k_3, $k_{4,\text{MeCN}}$, $(k_s/(k_s + k_b))_{\text{MeCN}}$, and $(k_s/(k_s + k_b))$ where the inequalities of the first three terms derived earlier served as initial guesses and fitting constraints. By using the measured quenching rate constant k_4 for cyclohexane and the quantum efficiency for the formation of **3**, $\phi_{\mathbf{3}} = 0.5$, as fixed parameters, the fit yielded the values $k_3 = 1.32 \times 10^7\ s^{-1}$, $k_{4,\text{MeCN}} = 6.65 \times 10^4\ M^{-1}\ s^{-1}$, $(k_s/(k_s + k_b))_{\text{MeCN}} = 0.784$, and for cyclohexane $k_s/(k_s + k_b) = 0.930$. The $\Phi_{\mathbf{H4}}^{-1}$ vs $[Q]^{-1}$ curves of all other substrates were each fit for the adjustable parameter, $k_s/(k_s + k_b)$, holding the above values for k_3, $k_{4,\text{MeCN}}$, and $(k_s/(k_s + k_b))_{\text{MeCN}}$ fixed (Table 2), as is illustrated in Figure 7 for both protiated and deuterated cyclohexane. The excellent fits obtained upon correction for quenching by MeCN make this method superior for estimating $\Phi_{\mathbf{H4},\text{lim}}$ relative to fitting "linear" portions of the $\Phi_{\mathbf{H4}}^{-1}$ vs $[Q]^{-1}$ curves. In particular, for cyclopentane and cyclohexane-d_{12}, the $\Phi_{\mathbf{H4},\text{app-lim}}$ values of 0.35 and 0.26 were corrected to 0.50 and 0.44, respectively.

Thus, $\Phi_{\mathbf{H4},\text{lim}}$ values for 2-butanol and all the cycloalkanes are nearly equal within experimental error and are all close to the theoretical maximum dictated by the quantum efficiency for the formation of **3**, $\phi_{\mathbf{3}} = 0.5$. Consequently, k_b must be significantly slower than k_s within the geminate radical pairs, {**H4**- -S•}, which is consistent with the expected large anodic shift in the oxidation potential of **H4** relative to **4**.[20] This leads to thermodynamic suppression of either back electron transfer or hydrogen atom transfer.

Since the decay of **H4** generated from the flash excitation of Na_4**1** in the presence of each of the cycloalkanes exhibits little changes up to 1 ms, and since the "instantaneous" quantum yields observed under continuous irradiation[19,20] are much lower than those reported here (Table 4), the back-reaction between the cycloalkyl radicals and either **H4** or **4** (derived from deprotonation of **H4**) must occur on a time scale much slower than 1 ms. Furthermore, the differences in product selectivities and yields observed under continuous irradiation must derive in part from differences in these slow back reactions. Although this comparison should be viewed with caution, it hints that **H4** may protect the radical from disproportionation and/or combination reactions, which are often both activationless and diffusion-controlled.[56]

Conclusions

Spectroscopic and kinetic evidence demonstrate that **3** is the key intermediate in oxidations photocatalyzed by M_4**1** and that **3** is a "hot" ground-state isomer with substantial O → W charge-transfer character. Although the rates for single electron transfer from neutral electron donors to **3** are nearly diffusion controlled, product accumulation is inefficient because slow separation of the geminate ion pair facilitates rapid back electron transfer. Product yields are improved if proton-transfer {**4**- -S−H•+} → {**H4**- -S•} suppresses the back-reaction or if either member of the ion-pair is scavenged by another reagent. Hydrocarbons and alcohols react with **3** by hydrogen atom transfer, producing high quantum yields of the geminate radical pairs {**H4**- -S•} and excitation of ground-state adducts {M_4**1**- -SH} is not required, as previously suggested. The reduction of the substrate-derived radical by **4** or **H4** must take place on a time scale slower than 1 ms.

Acknowledgment. This work was supported by the National Science Foundation and by the Texas Advanced Research Program.

Supporting Information Available: Transient absorbance (ΔA) kinetics representative of 300−380 nm behavior (detection of **2** and **3**); ΔA dependence on laser excitation energy; ΔA kinetics with different concentrations of DMPT and 2-butanol; microsecond time scale ΔA kinetics for the back-reaction **H4** + *cis*-1,2-dimethylcyclohexyl radical; plot of $\Phi_{\mathbf{H4}}^{-1}$ vs $[2\text{-butanol}]^{-1}$ (7 pages). See any current masthead page for ordering and Internet access instructions.

References and Notes

(1) Pope, M. T. *Heteropoly and Isopoly Oxometalates*; Springer-Verlag: Berlin, 1983.

(2) Pope, M. T.; Muller, A. *Angew. Chem., Int. Ed. Engl.* **1991**, *30*, 34.

(3) *Polyoxometalates: From Platonic Solids to Anti-retroviral Activity*; Pope, M. T., Muller, A., Eds.; Kluwer Academic Publishers: Dordrecht, The Netherlands, 1993.
(4) Papaconstantinou, E. *Chem. Soc. Rev.* **1989**, *18*, 1.
(5) The following special issue of *Chem. Rev.* is devoted to polyoxometalates: Guest Editor, C. L. Hill *Chem. Rev.* **1998**, *98*, 1.
(6) Hou, Y.; Hill, C. L. *New J. Chem.* **1992**, *16*, 909.
(7) Fox, M. A.; Cardona, R.; Gaillard, E. *J. Am. Chem. Soc.* **1987**, *109*, 6347.
(8) Kraut, B.; Ferraudi, G. *Inorg. Chem.* **1989**, *28*, 2692.
(9) Kraut, B.; Ferraudi, G. *Inorg. Chem.* **1990**, *29*, 4834.
(10) Nosaka, Y.; Takei, T.; Fujii, N. *J. Photochem. Photobiol. A: Chem.* **1995**, *92*, 173.
(11) Akid, R.; Darwent, J. R. *J. Chem. Soc., Dalton Trans.* **1985**, 395.
(12) Ward, M. D.; Brazdil, J. F.; Mehandu, S. P.; Anderson, A. B. *J. Phys. Chem.* **1987**, *91*, 6515.
(13) Combs-Walker, L. A.; Hill, C. L. *J. Am. Chem. Soc.* **1992**, *114*, 938.
(14) Maldotti, A.; Amadelli, R.; Varani, G.; Tollari, S.; Porta, F. *Inorg. Chem.* **1994**, *13*, 2968.
(15) Renneke, R.; Hill, C. L. *J. Am. Chem. Soc.* **1986**, *108*, 3528.
(16) Hill, C. L.; Renneke, R. F.; Combs, L. *Tetrahedron* **1988**, *44*, 7499.
(17) Hill, C. L.; Renneke, R. F.; Combs, L. A. *New J. Chem.* **1989**, *13*, 701.
(18) Renneke, R. F.; Hill, C. L. *Angew. Chem., Int. Ed. Engl.* **1988**, *27*, 1526.
(19) Renneke, R. F.; Pasquali, M.; Hill, C. L. *J. Am. Chem. Soc.* **1990**, *112*, 6585.
(20) Renneke, R. F.; Kadkhodayan, M.; Pasquali, M.; Hill, C. L. *J. Am. Chem. Soc.* **1991**, *113*, 8357.
(21) Hill, C. L.; Prosser-McCartha, C. M. In *Photosensitization and Photocatalysis Using Inorganic and Organometallic Complexes*; Kalyanasundaram, K., Gratzel, M., Eds.; Kluwer Academic Publishing: Dordrecht, The Netherlands, 1993; p 307.
(22) Yamase, T.; Usami, T. *J. Chem. Soc., Dalton Trans.* **1988**, 183.
(23) Duncan, D. C.; Netzel, T. L.; Hill, C. L. *Inorg. Chem.* **1995**, *34*, 4640.
(24) Prosser-McCartha, C. M.; Hill, C. L. *J. Am. Chem. Soc.* **1990**, *112*, 3671.
(25) Chemseddine, A.; Sanchez, C.; Livage, J.; Launay, J. P.; Fournier, M. *Inorg. Chem.* **1984**, *23*, 2609.
(26) Duncan, D. C.; Hill, C. L. *Inorg. Chem.* **1996**, *35*, 5828.
(27) Unfortunately, the spectrum of **H4** has not been reported owing to its rapid disproportionation to M_4**1** and $H_2[W_{10}O_{32}]^{4-}$.[1,33]
(28) Ermolenko, L. P.; Delaire, J. A.; Giannotti, C. *J. Chem. Soc., Perkin Trans. 2* **1997**, 25.
(29) Tanielian, C.; Duffy, K.; Jones, A. *J. Phys. Chem. B* **1997**, *101*, 4276.
(30) Hill, C. L.; Kozik, M.; Winkler, J.; Hou, Y.; Prosser-McCartha, C. M. In *Adv. Chem. Ser. "Photosensitive Metal-Organic Systems, Mechanistic Principles and Applications"*; Kutal, C., Serpone, N., Eds.; American Chemical Society: Washington, DC, 1993; Vol. 238; p 243.
(31) In ref 28, the authors did not observe the intermediate **2** at 380 nm.
(32) Previously, this transient has been assigned to $[W_{10}O_{32}]^{5-}$ **4**. Its decay has been claimed to be second order, and its yield reportedly increased with added cyclohexene.[22] However, our results and those in refs 23, 28, and 29 contradict these claims.
(33) Termes, S. C.; Pope, M. T. *Inorg. Chem.* **1978**, *17*, 500.
(34) Ratios above 1.14 are diagnostic of contamination by ψ-metatungstate and other colorless polyoxometalates.[26.]
(35) At laser energies between 15 and 40 mJ/pulse, plots of $\Delta A(t = 0)$ vs laser energy exhibit concave curvature with well-defined asymptotes at high laser energies (see Supporting Information). This is consistent with state saturation and is inconsistent with the onset of multiphoton processes. Furthermore, since the $t = 0$ transient (**3**, vide infra) has an intrinsic lifetime greater than 74 ns and absorbs little at 355 nm (Figure 1), stimulated emission must be an unimportant decay pathway. Since the decay lifetime is much longer than the 7 ns pulse width, the saturation asymptote observed in the plot of $\Delta A(t = 0)$ vs laser energy, $\Delta A = 0.148 \pm 0.005$, reflects a maximum conversion of M_4**1** to **3**.
(36) Hurley, J. K.; Sinai, N.; Linschitz, H. *Photochem. Photobiol.* **1983**, *38*, 9.
(37) For the photoreduction of M_4**1**, MeCN is the least reactive organic solvent known:[15] $\Phi = 0.004$ for Q_4**1** and $\Phi < 0.001$ for Na_4**1**.[19,20]
(38) The lifetimes of these transients are independent of the observation wavelength over the range 300−860 nm. However, within the <7 ns laser pulse duration, a transient observed between 300 and 380 nm (∼50% of the total absorbance) rises and decays with the contour of the laser pulse, indicating $\tau \ll 7$ ns (see Supporting Information). This component is assigned to the decay of **2** (Scheme 1) which has been detected previously, $\tau < 30$ ps.[23]
(39) In the study by Ermolenko et al.,[28] their lack of confirmation of the $\tau < 30$ ps transient **2** at 380 nm is puzzling. Nevertheless, a fast component derived from **2** clearly exists as is demonstrated in the transient behavior during the 7 ns pulse between 300 and 380 nm (see ref 38 and Supporting Information). Furthermore, they report no rising absorbance at 390 nm with added 0.025 M adamantane which was observed in ref 23 with either 0.5 M cyclohexene or 2 M 2-butanol. This is not surprising since more substrate would be needed to approach the quenching rates and product yields apparent in ref 23.
(40) Oxidation of **4** + **H4** by O_2 is observed for $t > 1$ μs and is reported in detail elsewhere.[28,29]
(41) For $M = Q^+$, the kinetics are complex and also exhibit a slower parallel second-order component, $k \sim 2 \times 10^8$ M^{-1} s^{-1}. In the calculation of [**4** + **H4**], the cell path length is approximated by the laser beam diameter, ∼0.7 cm.
(42) A small decrease in the transient absorbance is observed as the amine concentration is increased, possibly because of static quenching of **3** caused by association of the amine and **1** prior to excitation. NMR spectroscopic evidence has been reported for such an association between **1** and cyclohexylamine.[14]
(43) Schuler, R. H.; Patterson, L. K.; Janata, E. *J. Phys. Chem.* **1980**, *84*, 2088.
(44) The thiocyanate dimer radical anion, $[(SCN)_2]^{\bullet-}$, is a secondary product derived from the nearly quantitative and diffusion-controlled reaction between the thiocyanogen radical and thiocyanate.[43]
(45) Unfortunately, such high concentrations of either thianthrene or the three amines were precluded because of their weak electronic transitions ($n \rightarrow \pi^*$ and $l \rightarrow a_\pi$) which tail into the excitation wavelength, 355 nm. Consequently, their concentrations were limited to the 1−5 mM range, where control experiments indicated no excitation of these substrates. Indeed, this interference reduced the number of aromatic amine and thioether substrates available for study.
(46) Yamase, T. *J. Chem. Soc., Dalton Trans.* **1987**, 1597.
(47) The emission decays of polycrystalline polyoxometalates are complex,[48] consistent with inhomogeneous samples, and cannot be assigned with confidence.
(48) Yamase, T.; Sugeta, M. *J. Chem. Soc., Dalton Trans.* **1993**, 759.
(49) Robin, M. B.; Day, P. *Adv. Inorg. Chem. Radiochem.* **1967**, *10*, 247.
(50) Weinstock, I. A. *Chem. Rev.* **1998**, *98*, 113.
(51) Jen, S.-F.; Anderson, A. B.; Hill, C. L. *J. Phys. Chem.* **1992**, *96*, 5658.
(52) A primary kinetic isotope effect for quenching of **3** by MeCN/MeCN-d_3 is also evident but cannot be quantified since the intrinsic rate constant, k_3, is unknown (vide infra).
(53) With thiocyanate, the electrostatic repulsion of the encounter complex {**3**- -SCN^-} further reduces the rate of electron transfer.
(54) Determined from 0.0005/0.07, where 0.07 is the initial absorbance change.
(55) Sheldon, R. A.; Kochi, J. K. *Metal-Catalyzed Oxidations of Organic Compounds*; Academic Press: New York, 1981.
(56) Ingold, K. U. In *Free Radicals*; Kochi, J. K., Ed.; John Wiley & Sons: New York, 1973; Vol. 1.
(57) Bock, C. R.; Connor, J. A.; Gutierrez, A. R.; Meyer, T. J.; Whitten, D. G.; Sullivan, B. P.; Nagle, J. K. *J. Am. Chem. Soc.* **1979**, *101*, 4815.
(58) Connelly, N. G.; Geiger, W. E. *Chem. Rev.* **1996**, *96*, 877.